arXiv:1603.03746v1 [cond-mat.mtrl-sci] 11 Mar 2016

Unified Homogenization of Photonic/Phononic Crystals: Controllable First-band Negative Refraction

Sia Nemat-Nasser

Department of Mechanical and Aerospace Engineering
University of California, San Diego
La Jolla, CA, 92093-0416 USA

E-mail: sia@ucsd.edu

February 27, 2016

Abstract.

It is shown, for the first time, that negative refraction with positive phase velocity refraction can be realized (and controlled) over a wide range of frequency on the first (lowest) pass band of simple photonic and phononic crystals.

First a unified approach is presented to accurately, efficiently, and uniquely produce the homogenized effective material properties of doubly periodic phononic crystals for anti-plane shear (SH) and photonic crystals for transverse electric (TE) and transverse magnetic (TM) electromagnetic Bloch-form waves in such a manner that they exactly reproduce the band structure of the composite over any desired frequency band. Then the correspondence between phononic and photonic field equations is established and their effective homogenized material parameters are calculated. Finally illustrative examples are worked out for each case, revealing a rich body of refractive characteristics of these crystals, and showing by means of these examples that the homogenized effective parameters do yield the exact results, and that *the resulting homogenized medium does in fact embody exactly the actual band structure and dispersive properties of the considered phononic/photonic crystal.* As a consequence when the homogenized medium is placed in contact with a normal homogeneous half-space, *it could display, even on the first pass band, positive, negative, or even no energy refraction depending on the frequency and wave vector of plane waves incident from the normal homogeneous solid to the interface.*

The unit cell of the crystal may consist of anisotropic constituents of any constant or variable properties that may also admit large discontinuities. The actual calculation procedure is detailed in Appendix A, where, for elliptical and rectangular inclusion geometries, analytical expressions are also given to assist the calculation of the key quantities.

Keywords: First-band negative refraction; Effective dynamic properties; Doubly periodic phononic and photonic composites; Band structure, group and energy-flux vectors

1. Introduction

A representative volume element (RVE) of any heterogeneous material may be viewed as a unit cell of a periodic composite. But photonic and phononic crystals with their periodic arrangement of identical unit cells of structured constituent geometry and material properties, uniquely posses a wealth of special elastodynamic/electromagnetic characteristics that are not shared by an arbitrary RVE. These crystals display band structure and have dispersion responses that vary with frequency and wave vector, (Yablonovitch et al. 1991), (Plihal & Maradudin 1991), (Kushwaha et al. 1993), (Pendry 1994), (Sukhovich et al. 2008), (Nemat-Nasser 2015*a*), (Nemat-Nasser 2015*b*). The overall response of these crystals is fully defined by the geometry and material properties of their typical unit cell. Therefore, their homogenized effective properties for Bloch-form waves (Bloch 1928) can be calculated by simple spatial volume averaging of the field variables over a typical unit cell in such a manner that both continuity and periodicity are preserved. This approach was introduced in (Willis 2009), (Nemat-Nasser et al. 2011) for one-dimensional phononic crystals, and it is the approach we use in the present work. The resulting constitutive material parameters, obtained by this averaging scheme, together with the corresponding averaged field equations, will then by necessity produce the exact band structure of the original heterogeneous crystal. They are functions of the wave frequency and wave vector, are unique, and fully embody the refractive characteristics of the original composite. They may take on positive or negative values depending on the frequency and the wave vector. Hence the homogenized material may behave either as a normal composite or it may behave as a so-called metamaterial. We also show how this structure can be controlled and modified using anisotropic matrix materials and simple unit-cell geometries. We believe our results and the proposed method of analysis are new and should provide powerful tools for designing novel photonic or phononic crystals. Indeed, exploiting this, we show for the first time, that negative refraction with positive phase velocity refraction can be realized *and controlled on a wide frequency-range of the first (lowest) pass band* of simple photonic and phononic crystals.

Luo et al. (2002) have demonstrated negative refraction in a photonic crystal consisting of circular holes placed in a square-lattice pattern within a homogeneous and isotropic dielectric matrix. By interfacing the crystal with air along its (11)-direction, they observed that negative refraction for TE waves can occur in a narrow frequency (about 6.1%) at the far edges of the first pass band. In the present paper, we demonstrate a rich body of refractive characteristics that can be realized in photonic and phononic crystal over a wide region of the first pass band by suitably combining the square geometric anisotropy with material anisotropy, suggesting that this can be further enhanced by using a rectangular lattice structure.

An alternative method of homogenization is to consider a uniform reference medium with assumed constant properties and then introduce and calculate the necessary polarization strain-momentum or stress-velocity fields in the phononic case and

polarization electric and magnetic fields in the photonic case such as to produce pointwise the actual field variables. For elastodynamic and electromagnetic homogenization using this approach, Willis has developed general variational principles (Willis 1981*a*), (Willis 1981*b*), (Willis 1984) (Milton & Willis 2007). The polarization approach has also been used by (Amirkhizi & Nemat-Nasser 2008) to homogenize the electromagnetic properties of periodic media (photonic crystals), and by the present author and Srivastava (Nemat-Nasser & Srivastava 2011), (Srivastava & Nemat-Nasser 2012) to homogenize phononic crystals; see also (Srivastava 2015) for comments.

There are other methods for calculating the effective properties; see for example, (Joannopoulos et al. 2011), (Antonakakis et al. 2013*a*), (Antonakakis et al. 2013*b*), (Yang et al. 2014), (Antonakakis et al. 2014), (Yang et al. 2014), (Zhang & Wu 2015), and references cited therein. Here we use the direct field averaging for calculation of the effective properties that requires expressions of the periodic part of the field variables.

The accurate calculation of these periodic parts for two- and three-dimensional phononic/photonic crystals is a formidable task for unit cells consisting of constituents of diverse properties with discontinuities. Naturally, the accuracy of the final results, whether obtained by direct calculation or through the corresponding effective properties, will depend on the accuracy of the estimate of the periodic part of the field variables, though both methods will yield exactly the same results.

There are only limited computational tools that can be employed, each with its own limitations, (Leung & Liu 1990), (Bell et al. 1995), (Tran 1995), (Pendry 1996), (Birks et al. 2006), (Hussein 2009), (Nemat-Nasser 2015*b*). In the present work, we use a mixed variational formulation to calculate the band structure and the periodic part of the field variables (Nemat-Nasser 1972*a*). In this approach, both the displacement and stress fields in the phononic and the electric and magnetic fields in the photonic crystals are varied independently. Hence they may be approximated by any continuously differentiable set of complete base functions, even though in actuality the gradients of some of the field variables may suffer large discontinuities across interfaces of various constituents of a typical unit cell. Being based on a variational principle, any set of approximating functions can be used for the calculations, e.g., plane-wave Fourier series or finite elements (Nemat-Nasser et al. 1975), (Minagawa & Nemat-Nasser 1976), (Minagawa et al. 1981). The mix variational approach produces very accurate results and the rate of convergence of the corresponding series solution is superior to alternative methods (Babuška & Osborn 1978). The general approach has been used to develop a fast and accurate computational platform for band structure calculations (Lu & Srivastava 2016), where it is shown that this approach provides a greater convergence rate than the usual Rayleigh quotient, especially in the presence of large material discontinuities; see also (Nemat-Nasser 2015*a*) and (Nemat-Nasser 2015*b*).

2. Statement of the Problem and Field Equations

Consider a doubly periodic composite composed of rectangular unit cells of common dimensions a_1 and a_2. A typical unit cell, Ω_1, includes a nested set of concentric rectangular or elliptical (or their combination) shaped inclusions, Ω_l, $l = 2, 3, ..., n$, $\Omega_1 \supset \Omega_2 \supset \Omega_3 \ ... \supset \Omega_n$. For simplicity let the principal axes of the inclusions, $a_1(j)$ and $a_2(j)$, be parallel to the coordinate axes, x_1 and x_2, although this is not necessary. In what follows, we set $a_1 = a_1(1)$ and $a_2 = a_2(1)$.

We first consider the basic field equations and establish the one-to-one correspondence between anti-plane shear (SH) waves in phononic crystals and transverse electric (TE) and transverse magnetic (TM) electromagnetic (EM) waves in the photonic crystals. Then we present a general method to produce the homogenized constitutive parameters for the SH Bloch-waves by averaging the periodic part of the field variables and, based on the correspondence among the field variables, we summarize the results for the TE and TM, EM-waves. The calculation details are given in section (Appendix A). In section (4) we work out three numerical examples and also show that the homogenized effective medium does indeed embody the exact band structure of the original heterogeneous periodic composite, which clearly distinguishes it from any anisotropic normal material. We also show that negative refraction can occur on the first (acoustic) pass band.

2.1. Basic Field Equations: SH Waves

The Bloch-form SH waves of frequency ω involve two shear stresses, $\tau_j(x_1, x_2)$, $j = 1, 2$, and a lateral displacement, $w(x_1, x_2)$, satisfying the following field equations:

$$\begin{aligned} \tau_{j,j} + \omega^2 \rho w = 0, \quad \gamma_j = w_{,j}, \\ \tau_j = \mu_{jk}\gamma_k, \quad \gamma_j = D_{jk}\tau_k, \quad j, k = 1, 2. \end{aligned} \tag{1}$$

Here ρ is the mass density, $\mu_{jk} = \mu_{kj}$ and $D_{jk} = D_{kj}$ are the components of the shear and compliance moduli, respectively, repeated indices are summed, and a comma followed by an index denotes differentiation with respect to the corresponding coordinate variable. When the principal axes of the elasticity tensor, μ_{jk}, are in the x_1, x_2-directions, then $\mu_{12} = \mu_{21} = 0$. In what follows we consider the most general case where $\mu_{12} = \mu_{21} \neq 0$ and $\mu_{11} \neq \mu_{22}$, and show by means of illustrative examples how the resulting band structure is affected by these factors.

2.2. Basic Field Equations: TE/TM Waves

Consider now the basic equations for EM waves and denote by $\mathscr{E}_j$, $\mathscr{H}_j$, $\mathscr{B}_j$, and $\mathscr{D}_j$, $j = 1, 2, 3$, the components of electric, magnetic, magnetic induction, and electric displacement fields, respectively. Here we focus on TE and TM electromagnetic waves, set $\mathscr{E}_3 = \mathscr{H}_1 = \mathscr{H}_2 = 0$ and $\mathscr{H}_3 = \mathscr{H}$ for TE waves, and $\mathscr{H}_3 = \mathscr{E}_1 = \mathscr{E}_2 = 0$ and $\mathscr{E}_3 = \mathscr{E}$ for TM waves, reducing the general Maxwell equations,

$$\nabla \times \mathscr{E} - i\omega\mathscr{B} = 0, \quad \nabla \times \mathscr{H} + i\omega\mathscr{D} = 0, \tag{2}$$

$$\nabla.\,\mathscr{B} = \nabla.\,\mathscr{D} = 0, \quad \mathscr{D}_j = \epsilon_{jk}\mathscr{E}_k, \quad \mathscr{B}_j = \mu_{jk}\mathscr{H}_k, \tag{3}$$

to the following set of scalar equations, for TE and TM waves, respectively:

$$\begin{aligned} &\mathscr{E}_{1,2} - \mathscr{E}_{2,1} + i\omega\mu\mathscr{H} = 0,\\ &\mathscr{H}_{,2} + i\omega(\epsilon_{11}\mathscr{E}_1 + \epsilon_{12}\mathscr{E}_2) = 0,\\ &\mathscr{H}_{,1} - i\omega(\epsilon_{21}\mathscr{E}_1 + \epsilon_{22}\mathscr{E}_2) = 0 \quad , \end{aligned} \tag{4}$$

$$\begin{aligned} &-\mathscr{H}_{1,2} + \mathscr{H}_{2,1} + i\omega\epsilon\mathscr{E} = 0,\\ &\mathscr{E}_{,2} - i\omega(\mu_{11}\mathscr{H}_1 + \mu_{12}\mathscr{H}_2) = 0,\\ &\mathscr{E}_{,1} + i\omega(\mu_{21}\mathscr{H}_1 + \mu_{22}\mathscr{H}_2) = 0 \quad . \end{aligned} \tag{5}$$

In equations (4), $\mu = \mu_{33}$ is the magnetic permeability and $\epsilon_{jk} = \epsilon_{kj}$ are the components of the electric permittivity, and in equations (5), $\epsilon = \epsilon_{33}$ is the electric permittivity and $\mu_{jk} = \mu_{kj}$ are the components of the magnetic permeability, respectively. All the field variables are functions of x_1, x_2 only since the time variable is incorporated into the field equations. When the principal axes of the material parameters are, respectively, in the x_1, x_2-directions, then $\epsilon_{12} = \epsilon_{21} = 0$ and $\mu_{12} = \mu_{21} = 0$. Here again we do not assume this and consider the most general anisotropic case.

2.3. Correspondence between SH and TE/TM Waves

The field equations (4) reduce to field equations (1) if we set,

$$\mathscr{E}_1 = \tau_2, \quad \mathscr{E}_2 = -\tau_1, \quad \mathscr{H} = -i\omega w, \quad \mu = \rho, \quad \epsilon_{jk} = D_{jk}. \tag{6}$$

Similarly, the field equations (5) reduce to field equations (1) if we set,

$$\mathscr{H}_1 = -\tau_2, \quad \mathscr{H}_2 = \tau_1, \quad \mathscr{E} = -i\omega w, \quad \epsilon = \rho, \quad \mu_{jk} = D_{jk}. \tag{7}$$

Therefore, it is sufficient to outline the homogenization procedures for the SH stress waves and then extract the corresponding homogenized results for TE and TM waves by direct association based on equations (6) and (7).

To this end we average the periodic parts of the field equations as well as the periodic parts of the constitutive equations over a typical unit cell of the composite. In this manner the effective parameters are obtained independently of the conservation equations. Substitution of the resulting effective parameters into the averaged conservation relations should then yield the exact band structure in each case. The method in universal and can be used in two- and three-dimensional cases with impunity.

3. Homogenization

We now seek to extract the overall dynamic effective material parameters of the composite such that they produce the exact frequency band structure of the composite.

3.1. Homogenized Effective Parameters: SH Waves

For Bloch-form time-harmonic SH waves of frequency ω, traveling in a doubly periodic phononic crystal, the time-dependence of the field variables is incorporated into equations(1). These field variables have the following structure:

$$\begin{bmatrix} w \\ \gamma_j \\ \tau_j \end{bmatrix} = \begin{bmatrix} w^p(x_1,x_2) \\ \gamma_j^p(x_1,x_2) \\ \tau_j^p(x_1,x_2) \end{bmatrix} e^{i(k_1x_1+k_2x_2)}; \quad j=1,2, \tag{8}$$

where superimposed p denotes the periodic part, and k_1 and k_2 are the components of the wave vector.

3.1.1. Average Effective Constitutive Parameters: We directly average the periodic parts of equations (8) over a typical unit cell and set,

$$\begin{bmatrix} \bar{w} \\ \bar{\gamma}_j \\ \bar{\tau}_j \end{bmatrix} = \begin{bmatrix} \bar{w}^p \\ \bar{\gamma}_j^p \\ \bar{\tau}_j^p \end{bmatrix} e^{i(k_1x_1+k_2x_2)}; \quad j=1,2, \tag{9}$$

where a typical averaged field variable, say $\bar{G}$, is defined as

$$\bar{G} = \bar{G}^p e^{i(k_1x_1+k_2x_2)}, \qquad \bar{G}^p = \int_{-a_1/2}^{a_1/2}\int_{-a_2/2}^{a_2/2} G^p(x_1,x_2)dx_1x_2. \tag{10}$$

We now define the effective compliance and stiffness tensors, D_{jk}^{eff} and μ_{jk}^{eff}, and the effective mass density, ρ^{eff}, by

$$\overline{(D_{jk}\tau_k^p)} = D_{jk}^{eff}\bar{\tau}_k^p, \qquad \mu_{jk}^{eff} = [D_{jk}^{eff}]^{-1}, \qquad \overline{(\rho w^p)} = \rho^{eff}\bar{w}^p, \tag{11}$$

where the quantities $\overline{(D_{jk}\tau_k^p)}$ and $\overline{\rho w^p}$ are calculated by direct averaging over the unit cell. Using the averaged field quantities, (11), the field equations (1) are now averaged (see Appendix B for details) to obtain,

$$\begin{aligned} &ik_1\bar{\tau}_1 + ik_2\bar{\tau}_2 + \omega^2\rho^{eff}\bar{w} = 0, \quad ik_j\bar{w} - \bar{\gamma}_j = 0, \\ &\bar{\gamma}_j - D_{jk}^{eff}\bar{\tau}_k = 0, \quad \bar{\tau}_j - \mu_{jk}^{eff}\bar{\gamma}_k = 0, \quad [\mu_{jk}^{eff}] = [D_{jk}^{eff}]^{-1}. \end{aligned} \tag{12}$$

The band structure is obtained from equations (12) by substituting $(12)_{2,3,4}$ into $(12)_1$, arriving at,

$$\omega^2 = \frac{1}{\rho^{eff}}k_j\mu_{jl}^{eff}k_l, \quad j,l=1,2 \quad for\ SH,\ stress\ waves, \tag{13}$$

where the repeated indices are summed. Note that the effective compliance tensor, D_{jk}^{eff}, and hence the corresponding stiffness tensor, μ_{jk}^{eff}, as well as the effective mass density, ρ^{eff}, are calculated directly once the periodic parts of the stress and displacement fields are known. Although these fields are calculated independently using a mixed variational method, as discussed in Appendix A, they are the actual field quantities

that correspond to the exact associated frequency band. Therefore they should, by necessity, produce the correct band structure. It is however important to note that *the equation of motion*, $(12)_1$, *is not, and should not be used to obtain the effective constitutive parameters*. These effective parameters should characterize the considered particular material (here a linearly elastic one), independently of the conservation laws (here the linear momentum). The author has used a similar direct averaging technique to calculate the effective properties of phononic crystals in plane strain and plane stress cases where there are two coupled conservation equations. The procedure does indeed yield the exact band structure and the resulting effective compliance components do automatically satisfy the stress compatibility equation.

3.2. Homogenized Effective Parameters: TE/TM Waves

For the TE Bloch-form waves, set

$$\begin{bmatrix} \mathscr{H} \\ \mathscr{E}_j \end{bmatrix} = \begin{bmatrix} \mathscr{H}^p \\ \mathscr{E}_j^p \end{bmatrix} e^{i(k_1x_1+k_2x_2)}, \tag{14}$$

and for the TM Bloch-form waves, set

$$\begin{bmatrix} \mathscr{E} \\ \mathscr{H}_j \end{bmatrix} = \begin{bmatrix} \mathscr{E}^p \\ \mathscr{H}_j^p \end{bmatrix} e^{i(k_1x_1+k_2x_2)}. \tag{15}$$

Now consider equations (4,5), and following similar steps as before, obtain the following homogenized TE and TM wave equations, respectively:

$$\begin{aligned} &k_2\bar{\mathscr{E}}_1 - k_1\bar{\mathscr{E}}_2 + \omega\mu^{eff}\bar{\mathscr{H}} = 0,\\ &k_1\bar{\mathscr{H}} - \omega(\epsilon_{21}^{eff}\bar{\mathscr{E}}_1 + \epsilon_{22}^{eff}\bar{\mathscr{E}}_2) = 0,\\ &k_2\bar{\mathscr{H}} + \omega(\epsilon_{11}^{eff}\bar{\mathscr{E}}_1 + \epsilon_{12}^{eff}\bar{\mathscr{E}}_2) = 0; \end{aligned} \tag{16}$$

$$\begin{aligned} &k_1\bar{\mathscr{H}}_2 - k_2\bar{\mathscr{H}}_1 + \omega\epsilon^{eff}\bar{\mathscr{E}} = 0,\\ &k_2\bar{\mathscr{E}} - \omega(\mu_{11}^{eff}\mathscr{H}_1 + \mu_{12}^{eff}\mathscr{H}_2) = 0,\\ &k_1\bar{\mathscr{E}} + \omega(\mu_{21}^{eff}\bar{\mathscr{H}}_1 + \mu_{22}^{eff}\bar{\mathscr{H}}_2) = 0, \end{aligned} \tag{17}$$

where superimposed bar denotes the average value of the corresponding quantity, taken over a unit cell, and the effective properties for the TE and TM waves are defined such that,

$$\overline{(\mu\mathscr{H}^p)} = \mu^{eff}\bar{\mathscr{H}}^p, \quad \overline{(\epsilon_{jk}\mathscr{E}_k^p)} = \epsilon_{jk}^{eff}\bar{\mathscr{E}}_k^p, \quad [\nu_{jk}^{eff}] = [\epsilon_{jk}^{eff}]^{-1}, \quad for\ TE,\ EM\ waves; \tag{18}$$

$$\overline{(\epsilon\mathscr{E}^p)} = \epsilon^{eff}\bar{\mathscr{E}}^p, \quad \overline{(\mu_{jk}\mathscr{H}_k^p)} = \mu_{jk}^{eff}\bar{\mathscr{H}}_k^p, \quad [\lambda_{jk}^{eff}] = [\mu_{jk}^{eff}]^{-1}, \quad for\ TM,\ EM\ waves. \tag{19}$$

To express the band structure of the photonic crystal in terms of the corresponding effective properties, we combine equations (16 to 19) and obtain,

$$\omega^2 = \frac{1}{\mu^{eff}}(k_2^2\nu_{11}^{eff} + k_1^2\nu_{22}^{eff} - k_2k_1(\nu_{12}^{eff} + \nu_{21}^{eff})), \quad for\ TE,\ EM\ waves; \tag{20}$$

$$\omega^2 = \frac{1}{\epsilon^{eff}}(k_2^2\lambda_{11}^{eff} + k_1^2\lambda_{22}^{eff} - k_2k_1(\lambda_{12}^{eff} + \lambda_{21}^{eff})), \quad for\ TM,\ EM\ waves. \tag{21}$$

For numerical examples, we first calculate the field variables associated with each frequency band, and then, follow the procedure outlined above, appropriately average over a unit cell to obtain the effective parameters.

4. Illustrative Examples

We consider a simple two-phase photonic crystal that consists of a homogeneous anisotropic dielectric matrix containing 1.5mm holes, periodically spaced 4mm apart in both the x_1- and x_2-directions. Using thermoplastic co-extrusion fabrication or other methods, low-loss dielectric composites of various degrees of anisotropy can be fabricated; see, e.g., (Zhang et al. 2008), (Wing et al. 2006). Here, for illustration, we use a matrix with dielectric constants of $\epsilon_I^M = 9.6$ and $\epsilon_{II}^M = 90$, where the superimposed M denotes the matrix dielectric tensor.

To examine the effect of the microstructure of the unit cell on the response of the resulting medium, we consider two cases that differ from one another only by a different arrangement of the principal axes of the matrix dielectric tensors relative to the x_1, x_2-coordinate directions, i.e., in relation to the periodicity of the original composite. These cases are:

Case A: The principal axes of ϵ_{jk}^M coincide with the x_1, x_2-axes;

Case B: The principal axes of ϵ_{jk}^M make a 15^o angle with the x_1, x_2-axes.

We then show how the refractive behavior of the composite has been dramatically changed by this simple rearrangement. Indeed, *we show, for the first time, that even on the first (lowest) pass band of the medium, one can realize negative refraction over a broad range of frequencies and phase angles.* In addition, we show that the frequencies at which such response occurs can be lowered by surrounding the central hole with 0.5mm thick high-dielectric material; such high dielectric solids can be produced by various means, see, e.g., (Sengupta & Sengupta 1999), (Si et al. 2002).

In addition to the above two- and three-phase *photonic* composites, we also consider a very simple *phononic* crystal to illustrate our general results and show that negative energy refraction with positive phase-velocity refraction can be realized on the first (lowest) pass band. The constituent properties of the phononic crystal are chosen to have large variations within the unit cell to also show the effectiveness of the variational approach. These examples show the rich body of physics that can be revealed by the present approach as well as the versatility and effectiveness of the proposed computational tool; see also (Nemat-Nasser 2015*b*).

4.1. Unit-cell Properties for Photonic Crystal: TE-waves

Figures (1) show the unit cells of the two photonic crystals that are examined below. The arrows on the upper left corner of each unit cell indicate the directions of the principal

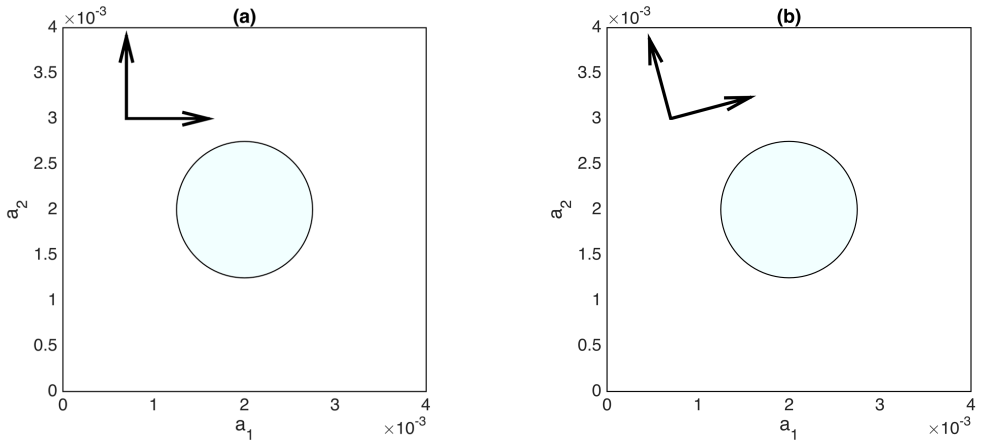

Figure 1. The unit cell of a two-phase photonic crystal consisting of an anisotropic matrix with a central hole. (a): The principal axes (heavy arrows) of ϵ_{jk}^M coincide with the x_1, x_2-axes; and (b): The principal axes (heavy arrows) of ϵ_{jk}^M make a 15^o angle with the x_1, x_2-axes.

axes of the dielectric tensor of the matrix material. In Figure (1a) these principal axes coincide with the x_1, x_2-axes, whereas in Figure (1b) they are at a 15^o angle with respect to the x_1, x_2-axes. The normalized wave-vector components are $Q_1 = a_1 k_1$ and $Q_2 = a_2 k_2$; note that $a_1 = a_2 = 4mm$ in the present case.

The matrix electric constants in Figure (1a) are:

- $\epsilon_{11}^M = 9.6$;
- $\epsilon_{22}^M = 90$;
- $\epsilon_{12}^M = \epsilon_{12}^M = 0$;
- $\mu^M = 1$.

The dielectric tensor for Figure (1b), with the same principal values as in Figure (1a), has the following components with respect to the x_1, x_2-coordinates:

- $\epsilon_{11}^M = 15$;
- $\epsilon_{22}^M = 84.6$;
- $\epsilon_{12}^M = \epsilon_{12}^M = 20.1$,

with $\mu^M = 1$.

The first 10 pass bands corresponding to these unit cells are shown in Figures 2 for $Q_2 = 1.07$. In these figures, the solid lines are obtained by direct band structure calculation using equation $(\text{A.10})_1$ whereas the open circles are by using the effective parameters; equation (20). As can be seen, the effective parameters yield the exact band structure in each case. In what follows, the effective parameters are used for all related calculations.

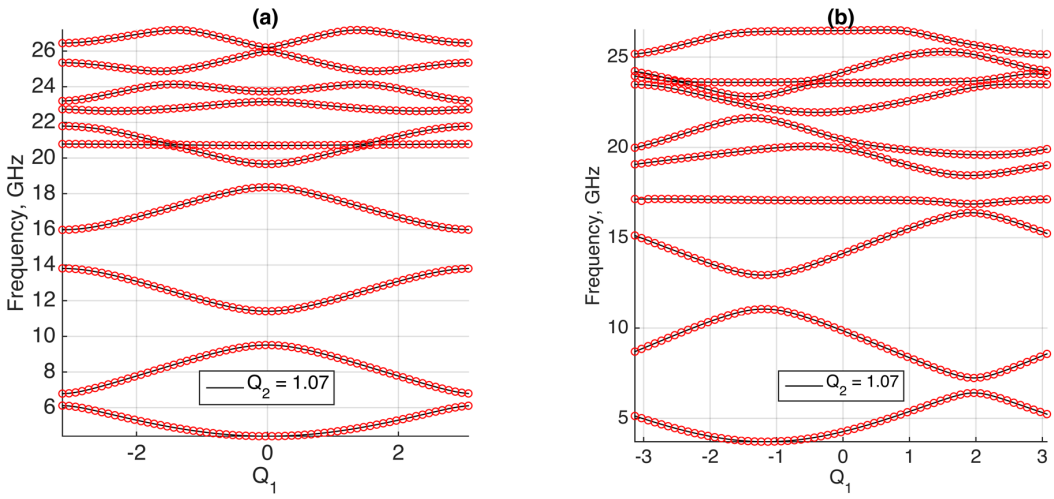

Figure 2. The first ten pass bands for $Q_2 = 1.07$; solid lines are by direct calculation using equations $(A.10)_1$; open circles are by homogenized parameters using equation (20). (a): Principal axes of electric permittivity tensor of matrix material coincide; (b): they are at about 15^o angle with respect to the x_1, x_2-axes; two-phase photonic crystal of unit cells shown in Figures (1a,b).

In Figures (3) we have shown the equi-frequency contours of the first three pass bands of these photonic crystals, calculated using the homogenized parameters. Identical results are obtained from the direct calculations.

The graphs in the left column in Figures 3 are for the case when the principal axes of the electric permittivity tensor of the matrix material coincide with the geometric symmetry axes of the periodic composite, and those on the right are for the case when the electric permittivity and the geometric principal axes are at about 15^o angle relative to one another.

The energy-flux vectors are also shown for these pass bands in Figures 3. As is well-known, the group velocity vector, v_j^g, and the energy-flux (Poynting) vector are coincident for the present class of problems, both pointing in the direction of energy flow. On each frequency band, J, the phase, v_{Jj}^p, and group, v_{Jj}^g, velocities are given by,

$$v_{Jj}^p = \frac{\omega_J k_j}{k_1^2 + k_2^2}, \quad v_{Jj}^g = \frac{\partial \omega_J}{\partial k_j}, \quad j = 1, 2; \tag{22}$$

here, $J = 1, 2, ...$ denotes the frequency band and $j = 1, 2$. At each point on a frequency contour in Figures (3), one can readily identify the direction of the energy flow and the corresponding direction of the phase velocity.

As is seen, when the principal axes of the matrix dielectric tensor coincide with the x_1, x_2-axes, we see on the first pass band the group velocity vectors pointing outwards on the first quadrant, indicating positive refraction for both the phase velocity and the group velocity (energy flux).

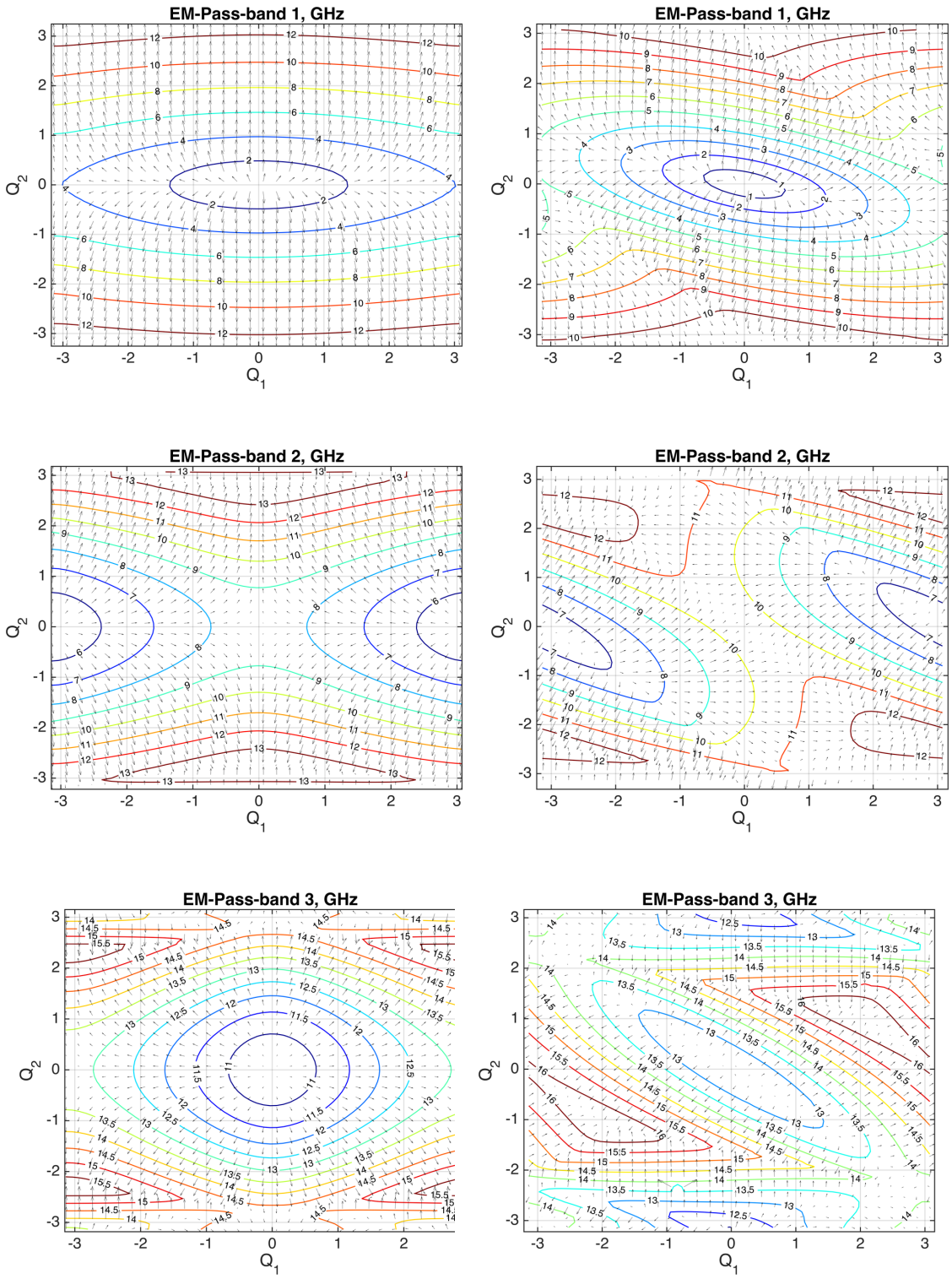

Figure 3. Equi-frequency contours of the first three pass bands of the photonic crystals Figures (1a,b). Principal axes of electric permittivity tensor of matrix material coincide (Left column), are at about 15^o angle (Right column) with the coordinate axes; arrows are the energy-flux vectors.

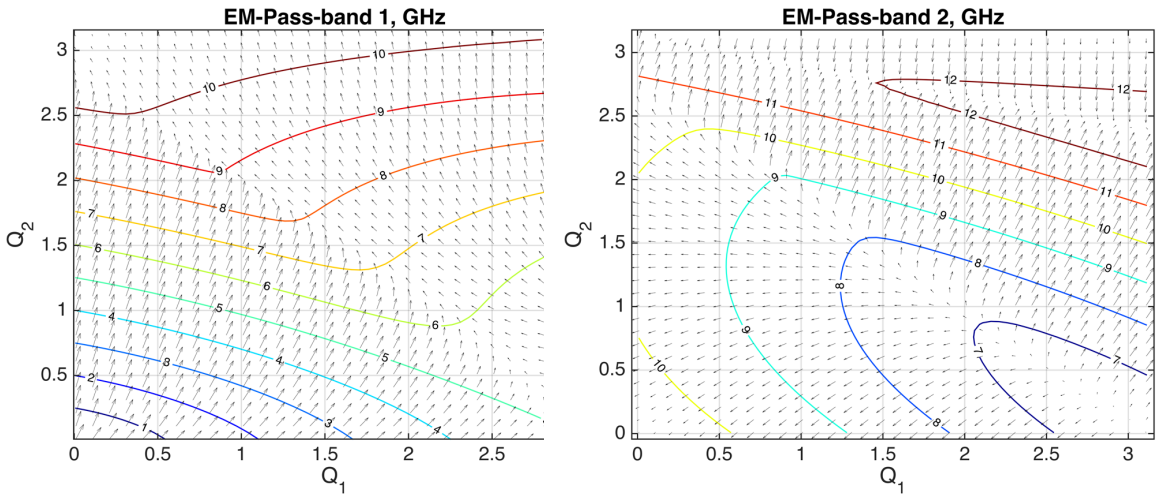

Figure 4. Equi-frequency contours and energy-flux vectors of the first two pass bands of a photonic crystal with unit cell shown in Figure (1b) for normalized wave vectors in the range $0 < Q_1, Q_2 < \pi$; arrows are the energy-flux vectors.

Here however, for the first time, without introducing a loaded series of capacitance and inductance (Siddiqui et al. 2003), we have realized negative energy refraction with positive phase-velocity refraction on a wide region of the first (lowest) frequency pass band of a photonic crystal of very simple unit cell: an anisotropic matrix with a central hole. In the past, negative refraction has been reported on the second pass band of periodic composites, similar to what is seen on the second band in the left column graphs of Figures (3). Here, even the second pass band in the right column graphs of Figures (3) embodies a rich variety of refractive characteristics, including positive refraction over a broad range of frequencies. These new results are better seen in Figures (4) on the first (left) and second (right) pass bands of the unit cell in Figure (1b) for the normalized wave vector in the range $0 < Q_1, Q_2 < \pi$.

4.2. Three-phase Composite

The computational tool presented in this paper allows to efficiently and accurately design unit cell for any desired refractive objectives. The available variables are the geometry of the unit cell, its composition, and in the present case the orientation of the principal axes of the matrix relative to the geometric symmetry of the unit cell. To illustrate this possibility, we modifying the above-considered unit cell by encasing the central circular hole with a 0.5mm material of high dielectric constant, say, $\epsilon_{11} = \epsilon_{22} = 150$, keeping all other parameters the same. Dielectric solids with very high dielectric constant have been fabricated; see, e.g., (Sengupta & Sengupta 1999), (Si et al. 2002). The corresponding unit cell and a portion of the first pass band are shown in Figures (5) for $0 < Q_1, Q_2 < \pi$. As is seen the frequencies are reduced by about 20%.

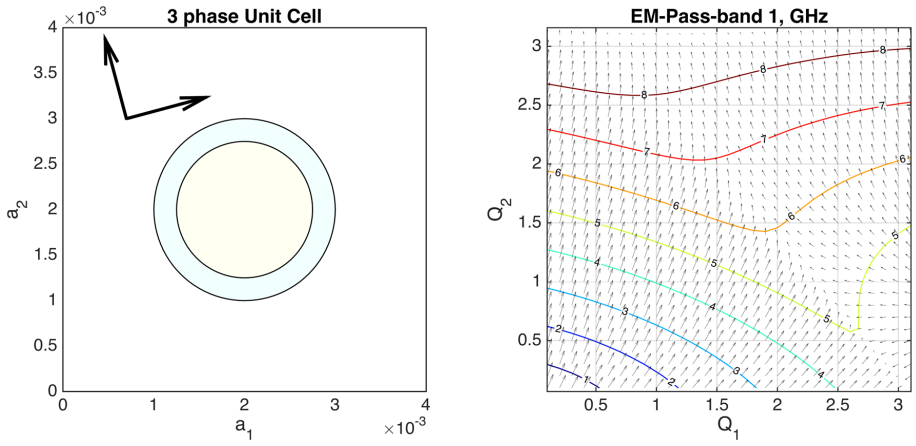

Figure 5. (Left): Unit cell of a three-phase photonic crystal consisting of an anisotropic matrix with a 0.5mm high-dielectric material surrounding the central circular hole; (Right): the first pass band for $0 < Q_1, Q_2 < \pi$. Principal axes of electric permittivity tensor of the matrix (Left, heavy arrows) are at about 15^o angle with respect to the x_1, x_2-coordinate axes.

4.3. Unit-cell Properties for Phononic Crystal; SH-waves

We consider a simple two-phase phononic crystal with the unit cell shown in Figure (6a). It consists of a unidirectionally reinforced carbon fiber-epoxy composite matrix containing 2mm-diameter circular aluminum-inclusions that are spaced 5mm center-to-center in the x_1 and x_2-directions such that the principal directions of the matrix stiffness tensor make a 30^o angle with the x_1, x_2-axis, as shown by the arrows in Figure (6a). The principal values of the shear modulus tensor are measured at 500kHz to be $\mu_I^M = 2.4GPa$ and $\mu_{II}^M = 5.8GPa$. The corresponding components in the x_1, x_2-coordinates, and the properties of the aluminum inclusions are,

(i) μ_{11}^M=3.25GPa; μ_{22}^M=4.95GPa; μ_{12}^M=1.47GPa; ρ^M=1440kg/m^3.
(ii) $\mu_{11}^{In} = \mu_{22}^{In}$=28GPa; ρ^{In}=2700kg/m^3.

The first ten pass bands of this crystal are shown in Figure (6b) for $Q_2 = 1.06$, and in Figure (7) we have shown the equi-frequency contours of the first four pass bands. The arrows in the contour maps are the corresponding energy-flux vectors.

As is evident from the energy-flux directions over the first (lowest) frequency pass band in Figure (7), negative refraction occurs with positive phase-velocity refraction over a wide range of positive phase angles. Indeed by simply suitably arranging the axes of the matrix anisotropy relative to the x_1, x_2-axes, a remarkably rich body of refraction characteristics of the composite is realized. We believe these results and our proposed method of analysis are new, and should provide powerful tools for designing novel phononic crystals. In Figures (8) we have captured the refraction response of this simple phononic crystal for the indicated values of the wave-vector components over

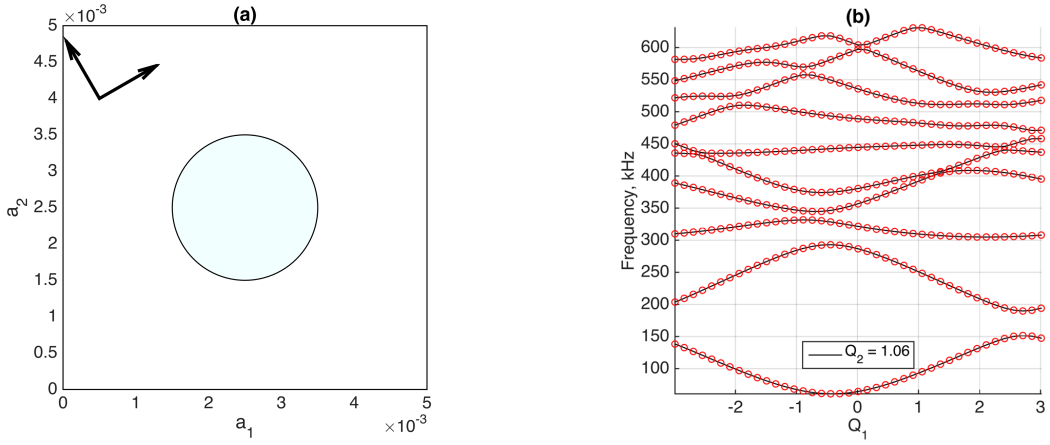

Figure 6. (a): A two-phase phononic crystal. (b): The first ten pass bands for $Q_2 = 1.06$; solid lines are by direct calculation using equations (A.5); open circles are by homogenized parameters using equation (13).

the first two (lowest two) pass bands where the phase velocity is positive. Positive or negative energy refraction is captured at various frequencies.

5. Discussion and Conclusions

We have shown, for the first time, that negative refraction with positive phase velocity refraction can be realized over a broad range of frequencies on the first (lowest) frequency pass band of very simple photonic and phononic crystals, and that this can be controlled by suitable unit-cell design.

First we have provided a unified methodology to accurately and efficiently produce the homogenized effective material properties of doubly periodic phononic crystals for anti-plane shear (SH) and photonic crystals for transverse electric (TE) and transverse magnetic (TM) electromagnetic Bloch-form waves over any desired range of frequencies. We have shown the correspondence between phononic and photonic field equations, and have outlined in detail the actual calculation procedures. We have worked out illustrative examples for each case and have unveiled a rich body of refractive characteristics of these crystals that have thus far been hidden.

It turns out that both photonic and phononic crystals with even the simplest unit

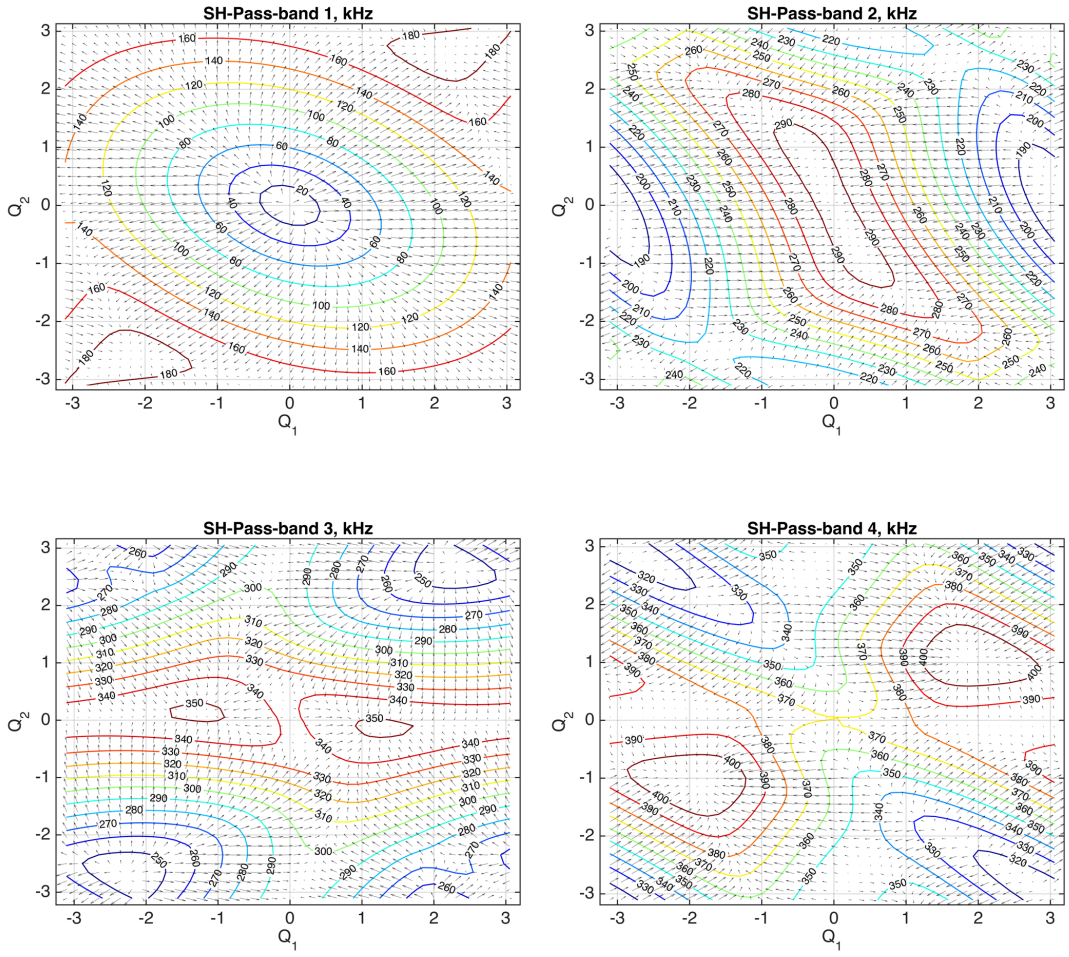

Figure 7. Equi-frequency contours of the first four pass bands of the phononic crystal Figure (6a); arrows are the energy-flux vectors.

cells have a rich body of refractive responses that can be realized even on the first (lowest) frequency pass band. Indeed, on the first and second frequency pass bands, one can have: (a) negative refraction with negative phase-velocity refraction, (b) negative refraction with positive phase-velocity refraction, (c) positive refraction with negative phase-velocity refraction, (d) positive refraction with positive phase-velocity refraction, or even (e) complete reflection with no energy transmission, depending on the frequency and wave vector.

Our calculation method applies to any unit cell that may consist of anisotropic constituents of any constant or variable properties that may also admit large discontinuities. The homogenized (spatially constant) effective material parameters depend parametrically on the wave frequency and wave vector. *They embody the actual dispersive properties of the considered phononic/photonic crystal, and produce their exact band structure.* Using the same volume fraction of the same constituents,

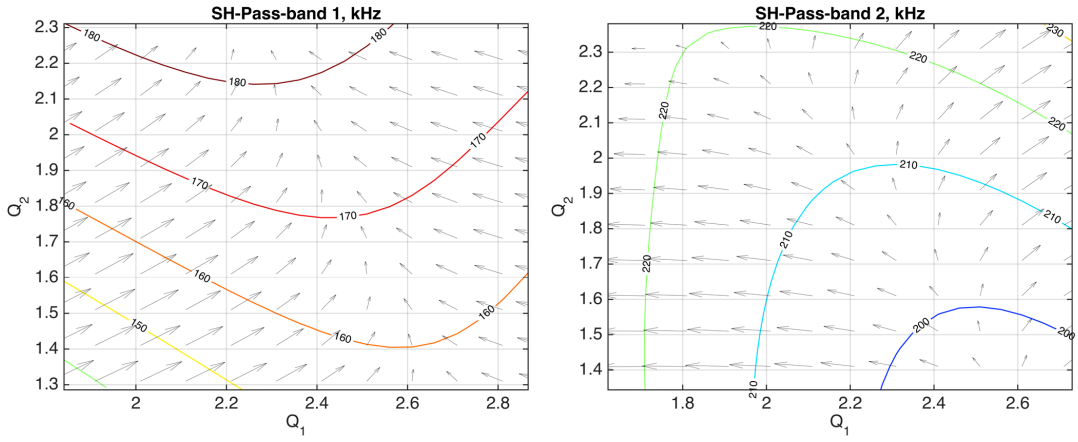

Figure 8. Equi-frequency contours of phononic crystal with unit cell shown in Figure (6a) for indicated values of the wave-vector components over the first two (lowest two) pass bands where the phase velocity is positive; arrows are the energy-flux vectors.

one can design a (homogenized) material that would display negative energy refraction with positive phase velocity refraction even on its first (acoustic) pass band, providing opportunity for a variety of applications where devices with low loss refractive properties are required. The window of frequency and the range of wave-vector values at which the negative energy refraction would occur can be controlled by judicious selection and design of the unit cell's constituent geometry and properties.

Acknowledgments: This research has been conducted at the Center of Excellence for Advanced Materials (CEAM) at the University of California, San Diego, under DARPA RDECOM W91CRB-10-1-0006 to the University of California, San Diego.

Appendix A. Band Structure Calculation

The calculation of the band structure and the associated field variables for two- and three-dimensional phononic/photonic crystals presents a formidable challenge especially when their unit cells consist of constituents of diverse properties with large discontinuities. There are limited computational tools that can be employed, each with its own limitations, see for example the following and cited references therein: (Leung & Liu 1990), (Plihal & Maradudin 1991), (Kushwaha et al. 1993), (Pendry 1994), (Bell et al. 1995), (Tran 1995), (Pendry 1996), (Chou & Lin 2014), (Han & Chang 2014). In the present work, we use a mixed variational formulation for band-structure calculations, where both the displacement and stress fields in the phononic and the electric and magnetic fields in the photonic crystals are varied independently. Hence they may be approximated by any continuously differentiable set of complete base functions, even though the gradients of some of the field variables may suffer large discontinuities across

interfaces of various constituents of a typical unit cell. Since the method is based on a variational principle, any set of approximating functions can be used for calculations, e.g., plane-wave Fourier series or finite elements (Nemat-Nasser et al. 1975), (Minagawa & Nemat-Nasser 1976), (Minagawa et al. 1981). The mixed variational produces very accurate results and the rate of convergence of the corresponding series solution is superior to alternative methods (Babuška & Osborn 1978). The general approach has been used to develop a fast and accurate computational platform for band structure calculations (Lu & Srivastava 2016), where it is also shown that the mixed variational approach provides greater convergence rate than the usual Rayleigh quotient, especially in the presence of large material discontinuities. Other variational methods have also been used for band structure calculation of periodic composites, see, e.g., (Goffaux & Sánchez-Dehesa 2003).

In what follows, detailed calculations are given for the SH waves and then the results for TE and TM waves are extracted using the corresponding equations.

Appendix A.1. SH Waves

We minimize the following functional, considering the displacement and stresses as independent fields subject to variation:

$$\omega^2 = \frac{< \tau_j, w_{,j} > + < w_{,j}, \tau_j > - < D_{jk}\tau_k, \tau_j >}{< \rho w, w >}; \quad j,k = 1,2, \tag{A.1}$$

where $< gu, v >= \int_{-1/2}^{1/2}\int_{-1/2}^{1/2} guv^* dx_1 dx_2$ for a real-valued function $g(x_1, x_2)$ and complex-valued functions $u(x_1, x_2)$ and $v(x_1, x_2)$, with star denoting complex conjugate, the repeated indexes being summed.

The functional (A.1) was introduced by the present author in the early 1970's (Nemat-Nasser (1972*b*)) and was termed *new quotient*. It yields remarkably accurate frequency bands of phononic crystals using only a few plane-wave approximations as compared with the usual Rayleigh quotient (Nemat-Nasser 2015*b*). Here we use the following approximating functions:

$$\begin{bmatrix} w \\ \tau_j \end{bmatrix} = \sum_{n_1,n_2=-N}^{+N} \begin{bmatrix} W^{n_1 n_2} \\ T_j^{n_1 n_2} \end{bmatrix} e^{i[(k_1+\frac{2\pi n_1}{a_1})x_1+(k_2+\frac{2\pi n_2}{a_2})x_2]}, \tag{A.2}$$

which automatically ensures the Bloch and continuity conditions, and, by direct substitution into (A.1) and minimization with respect to W and T_j as the independent variables, obtain

$$\begin{bmatrix} iH_1 & iH_2 & \omega^2\Lambda_\rho \\ \Lambda_{D_{11}} & \Lambda_{D_{12}} & -iH_1 \\ \Lambda_{D_{21}} & \Lambda_{D_{22}} & -iH_2 \end{bmatrix} \begin{bmatrix} T_1 \\ T_2 \\ W \end{bmatrix} = 0, \tag{A.3}$$

where $\Lambda_f = [\Lambda_f^{(n_1 n_2, m_1 m_2)}]$ is an $M^2 \times M^2$ matrix, and H_1 and H_2 are two $M^2 \times M^2$ diagonal matrices with the respective components $(k_1 + 2\pi n_1)\delta_{n_1 m_1}\delta_{n_2 m_2}$ and $(k_2 +$

$2\pi n_2)\delta_{n_1m_1}\delta_{n_2m_2}$, where $M = 2N + 1$. The components of Λ_f are defined by

$$\Lambda_f^{(n_1n_2,m_1m_2)} = \int_{-a_1/2}^{a_1/2}\int_{-a_2/2}^{a_2/2} f(x_1,x_2)e^{i2\pi[(n_1-m_1)x_1+(n_2-m_2)x_2]}dx_1dx_2, \tag{A.4}$$

with $f(x_1, x_2)$ being a real-valued integrable function. For an even function, $f(x_1, x_2) = f(-x_1, -x_2)$ (symmetric unit cells), and $\Lambda_f^{(n_1n_2,m_1m_2)} = \Lambda_f^{(m_1m_2,n_1n_2)}$ is real-valued.

From the system of linear and homogeneous equations (A.3),we obtain,

$$[\Phi - \omega^2\Omega]\,W = 0, \quad \Omega = \Lambda_\rho, \quad \Phi = H_jM_{jk}H_k, \quad [M_{jk}] = \left[\Lambda_{D_{jk}}\right]^{-1}, \tag{A.5}$$

where $j, k = 1, 2$, and repeated indices are summed. For given values of k_1 and k_2, the eigenvalues, ω, of equation$(A.5)_1$ are obtained from

$$det\left|\Phi - \omega^2\Omega\right| = 0, \tag{A.6}$$

and for each eigenvalue, the corresponding $M \times M$ displacement matrix, $W = [W^{n_1n_2}]$, is given by $(A.5)_1$, and the stresses, $T_j = [T_j^{n_1n_2}]$, and strains, $\gamma_j = [\gamma_j^{n_1n_2}]$, by,

$$T_j = iM_{jk}H_kW, \quad \gamma_j = \Lambda_{D_{jk}}T_k, \quad \gamma_j = iH_jw. \tag{A.7}$$

Appendix A.2. TE/TM Waves

For the TE Bloch-form waves, set

$$\begin{bmatrix} \mathscr{H} \\ \mathscr{E}_j \end{bmatrix} = \sum_{n_1,n_2=-N}^{+N} \begin{bmatrix} \mathscr{H}^{n_1n_2} \\ \mathscr{E}_j^{n_1n_2} \end{bmatrix} e^{i[(k_1+\frac{2\pi n_1}{a_1})x_1+(k_2+\frac{2\pi n_2}{a_2})x_2]}, \tag{A.8}$$

and for the TM Bloch-form waves, set

$$\begin{bmatrix} \mathscr{E} \\ \mathscr{H}_j \end{bmatrix} = \sum_{n_1,n_2=-N}^{+N} \begin{bmatrix} \mathscr{E}^{n_1n_2} \\ \mathscr{H}_j^{n_1n_2} \end{bmatrix} e^{i[(k_1+\frac{2\pi n_1}{a_1})x_1+(k_2+\frac{2\pi n_2}{a_2})x_2]}. \tag{A.9}$$

Then using the correspondence relations (6), we obtain, for TE-waves,

$$\begin{aligned} &[\Phi - \omega^2\Omega]\mathscr{H} = 0, \quad \Omega = \Lambda_\mu, \\ &\Phi = H_2\nu_{11}H_2 + H_1\nu_{22}H_1 - (H_2\nu_{12}H_1 + H_1\nu_{21}H_2), \\ &\mathscr{E}_1 = \tfrac{1}{\omega}(-\nu_{11}H_2 + \nu_{12}H_1)\mathscr{H}, \\ &\mathscr{E}_2 = \tfrac{1}{\omega}(-\nu_{21}H_2 + \nu_{22}H_1)\mathscr{H}; \quad [\nu_{jk}] = [\Lambda\epsilon_{jk}]^{-1}. \end{aligned} \tag{A.10}$$

Similarly, for TM-waves, we use (7) and obtain,

$$\begin{aligned} &[\Phi - \omega^2\Omega]\mathscr{E} = 0, \quad \Omega = \Lambda_\epsilon, \\ &\Phi = H_2\lambda_{11}H_2 + H_1\lambda_{22}H_1 - (H_1\lambda_{21}H_2 + H_2\lambda_{12}H_1)\mathscr{H}, \\ &\mathscr{H}_1 = \tfrac{1}{\omega}(\lambda_{11}H_2 - \lambda_{12}H_1)\mathscr{E}, \\ &\mathscr{H}_2 = \tfrac{1}{\omega}(\lambda_{21}H_2 - \lambda_{22}H_1)\mathscr{E}, \quad [\lambda_{jk}] = [\Lambda\mu_{jk}]^{-1}, \end{aligned} \tag{A.11}$$

where $\Lambda\epsilon_{jk}$ and $\Lambda\mu_{jk}$ are defined by equation (A.4); see also below.

Appendix A.3. Expressions for $\Lambda_{f(x_1,x_2)}$ in Special Cases

When a rectangular unit cell contains a nested sequence of either rectangular or elliptical inclusions, matrix $\Lambda_{f(x_1,x_2)}$ can be calculated explicitly for piecewise constant values of $f(x_1, x_2)$. Consider an a_1 by a_2 unit cell, Ω_1, that contains a nested sequence of $n-1$ concentric either elliptical or rectangular subregions, $\Omega_1 \supset \Omega_2 \supset \Omega_3 \ ... \supset \Omega_n$.

Denote the dimensions of the principal axes of a typical subregion Ω_j by $a_1(j)$ and $a_2(j)$. Then the area of the j^{th} subregion is $\Omega_j - \Omega_{j-1}$, where for a rectangular subregion $\Omega_j = a_1(j)a_2(j)$, and for an elliptical subregion $\Omega_j = \frac{\pi}{4}a_1(j)a_2(j)$. Let $f(j)$ stand for either the mass-density or the shear modulus of the subregion $\Omega_j - \Omega_{j-1}$. From (A.4) now obtain,

$$\Lambda_f = \sum_{k=2}^{n}(f_k - f_{k-1})g_k, \tag{A.12}$$

$$g_k = \int_{\Omega_k} exp\{i2\pi[(\frac{n_1 - m_1}{a_1})x_1 + (\frac{n_2 - m_2}{a_2})x_2]\}dx_1dx_2, \tag{A.13}$$

where for a rectangular subregion g_k is given by,

$$g_k = \begin{cases} \frac{sin(\pi nm_1 a_1(k)/a_1)}{\pi nm_1}\frac{sin(\pi nm_2 a_2(k)/a_2)}{\pi nm_2} & nm_1 \neq 0, \quad nm_2 \neq 0, \\ \frac{sin(\pi nm_1 a_1(k)/a_1)}{\pi nm_1 a_2}a_2(k) & nm_1 \neq 0, \quad nm_2 = 0, \\ \frac{sin(\pi nm_2 a_2(k))}{\pi nm_2 a_1}a_1(k) & nm_1 = 0, \quad nm_2 \neq 0, \\ \frac{a_1(k)a_2(k)}{a_1 a_2}, & nm_1 = 0, \quad nm_2 = 0, \\ nm_1 = n_1 - m_1, \ nm_2 = n_2 - m_2, & \\ (k \ not \ summed); & \end{cases} \tag{A.14}$$

and for an elliptical subregion g_k becomes,

$$g_k = \frac{\pi}{2}\frac{a_1(k)a_2(k)J_1(R_k)}{a_1 a_2 R_k}, \quad R_k = \pi\{[nm_1 a_1(k)/a_1]^2 + [nm_2 a_2(k)/a_2]^2\}^{1/2}. \tag{A.15}$$

Appendix A.4. Calculation of Effective Properties

The periodic part of the field variables is directly averaged to obtain the corresponding effective parameters according to equations (11) for SH waves and equations (18) and (19) for TE and TM. Here we give the equations for the calculation of the effective properties for SH-waves as illustration; similar equations hold for TE and TM, EM-waves,

$$\begin{aligned} \overline{(D_{jk}\tau_k)} &= D_{jk}^{eff}\bar{\tau}_k = \sum_{n_1,n_2=-N}^{+N} K^{n_1 n_2}[D_{jk}(\mathbf{x})]T_k^{n_1 n_2}, \quad \bar{\tau}_j = T_j^{00}, \\ \overline{(\rho w)} &= \sum_{n_1,n_2=-N}^{+N} K^{n_1 n_2}[\rho(\mathbf{x})]W^{n_1 n_2}, \quad \bar{w} = W^{00}, \end{aligned} \tag{A.16}$$

where

$$K^{n_1n_2}[f(\mathbf{x})] = K_{f(x_1,x_2)} = \int_{-a_1/2}^{a_1/2}\int_{-a_2/2}^{a_2/2} f(\mathbf{x})e^{i2\pi(\frac{n_1x_1}{a_1}+\frac{n_2x_2}{a_2})}dx_1dx_2. \tag{A.17}$$

As for $\Lambda_{f(x_1,x_2)}$, explicit expression can be obtained for $K_{f(x_1,x_2)}$ when a unit cell contains a nested sequence of elliptical or rectangular inclusion. Using a similar notation as in equation (A.12), we set,

$$K_f = \sum_{k=2}^{n}(f_k - f_{k-1})h_k, \tag{A.18}$$

$$h_k = \int_{\Omega_k} exp\{i2\pi[\frac{n_1x_1}{a_1} + \frac{n_2x_2}{a_2}]\}dx_1dx_2, \tag{A.19}$$

where for a rectangular subregion h_k is given by,

$$h_k = \begin{cases} \frac{sin(\pi n_1a_1(k)/a_1)}{\pi n_1}\frac{sin(\pi n_2a_2(k)/a_2)}{\pi n_2} & n_1 \neq 0, \quad n_2 \neq 0, \\ \frac{sin(\pi n_1a_1(k)/a_1)}{\pi n_1a_2}a_2(k) & n_1 \neq 0, \quad n_2 = 0, \\ \frac{sin(\pi n_2a_2(k))}{\pi n_2a_1}a_1(k) & n_1 = 0, \quad n_2 \neq 0, \\ \frac{a_1(k)a_2(k)}{a_1a_2}, & n_1 = 0, \quad n_2 = 0, \end{cases} \tag{A.20}$$

and for an elliptical subregion h_k becomes,

$$h_k = \frac{\pi}{2}\frac{a_1(k)a_2(k)J_1(R_k)}{a_1a_2R_k}, \quad R_k = \pi\{[n_1a_1(k)/a_1]^2 + [n_2a_2(k)/a_2]^2\}^{1/2}. \tag{A.21}$$

Appendix B. Averaging Procedure

Here we present the details of the averaging procedure. Consider the dynamic field equations (1) and, for notational simplicity, introduce the two-dimensional vectors, $\mathbf{k}, \mathbf{x}, \mathbf{X}$,and $\mathbf{y}$ with the respective components, k_j, x_j, X_j, and y_j. Now multiply $(1)_{1,2,3}$ by $e^{-i\mathbf{k}.\mathbf{X}}$ and write the resulting equations as,

$$\begin{aligned} &\frac{\partial}{\partial x_j}\big(\tau_j^p(\mathbf{x})e^{i\mathbf{k}.(\mathbf{x}-\mathbf{X})}\big) + \omega^2\rho(\mathbf{x})w^p(\mathbf{x})e^{i\mathbf{k}.(\mathbf{x}-\mathbf{X})} = 0, \\ &\frac{\partial}{\partial x_j}\big(w^p(\mathbf{x})e^{i\mathbf{k}.(\mathbf{x}-\mathbf{X})}\big) - \gamma_j^p(\mathbf{x})e^{i\mathbf{k}.(\mathbf{x}-\mathbf{X})} = 0, \\ &\tau_j^p(\mathbf{x})e^{i\mathbf{k}.(\mathbf{x}-\mathbf{X})} - \mu_{jk}(\mathbf{x})\gamma_k^p e^{i\mathbf{k}.(\mathbf{x}-\mathbf{X})} = 0, \\ &\gamma_j^p(\mathbf{x})e^{i\mathbf{k}.(\mathbf{x}-\mathbf{X})} - D_{jk}(\mathbf{x})\tau_k^p e^{i\mathbf{k}.(\mathbf{x}-\mathbf{X})} = 0, \end{aligned} \tag{B.1}$$

set $\mathbf{y} = \mathbf{x} - \mathbf{X}$ and obtain,

$$\begin{aligned} &\frac{\partial}{\partial y_j}\big(\tau_j^p(\mathbf{X}+\mathbf{y})e^{i\mathbf{k}.\mathbf{y}}\big) + \omega^2\rho(\mathbf{X}+\mathbf{y})\big(w^p(\mathbf{X}+\mathbf{y})e^{i\mathbf{k}.\mathbf{y}}\big) = 0, \\ &\frac{\partial}{\partial y_j}\big(w^p(\mathbf{X}+\mathbf{y})e^{i\mathbf{k}.\mathbf{y}}\big) - \gamma_j^p(\mathbf{X}+\mathbf{y})e^{i\mathbf{k}.\mathbf{y}} = 0, \\ &\tau_j^p(\mathbf{X}+\mathbf{y})e^{i\mathbf{k}.\mathbf{y}} - \mu_{jk}(\mathbf{X}+\mathbf{y})\gamma_k^p(\mathbf{X}+\mathbf{y})e^{i\mathbf{k}.\mathbf{y}} = 0, \\ &\gamma_j^p(\mathbf{X}+\mathbf{y})e^{i\mathbf{k}.\mathbf{y}} - D_{jk}(\mathbf{X}+\mathbf{y})\tau_k^p(\mathbf{X}+\mathbf{y})e^{i\mathbf{k}.\mathbf{y}} = 0. \end{aligned} \tag{B.2}$$

Finally average the field equations with respect to$\mathbf{X}$ over the unit cell and obtain,

$$\begin{aligned} &ik_1\bar{\tau}_1 + ik_2\bar{\tau}_2 + \omega^2\rho^{eff}\bar{w} = 0, \quad ik_j\bar{w} - \bar{\gamma}_j = 0, \\ &\bar{\tau}_j - \mu^{eff}_{jk}\bar{\gamma}_k = 0, \quad \bar{\gamma}_j - D^{eff}_{jk}\bar{\tau}_k = 0, \end{aligned} \tag{B.3}$$

where the superimposed bar stands for the averaged periodic part of the corresponding field variable, and definitions (11) are used.

Appendix C. References

Amirkhizi A V & Nemat-Nasser S 2008 *Smart Materials and Structures* **17**(1), 015042.

Antonakakis T, Craster R & Guenneau S 2013*a* *in* 'Proceedings of the Royal Society of London A: Mathematical, Physical and Engineering Sciences' Vol. 469 The Royal Society p. 20120533.

Antonakakis T, Craster R & Guenneau S 2013*b* *New Journal of Physics* **15**(10), 103014.

Antonakakis T, Craster R & Guenneau S 2014 *Journal of the Mechanics and Physics of Solids* **71**, 84–96.

Babuška I & Osborn J 1978 *Mathematics of Computation* **32**(144), 991–1023.

Bell P, Pendry J, Moreno L M & Ward A 1995 *Computer physics communications* **85**(2), 306–322.

Birks T A, Pearce G J & Bird D M 2006 *Optics express* **14**(20), 9483–9490.

Bloch F 1928 *Z. Phys* **52**, 555–600.

Chou S H & Lin W W 2014.

Goffaux C & Sánchez-Dehesa J 2003 *Physical Review B* **67**(14), 144301.

Han K & Chang C H 2014 *Nanomaterials* **4**(1), 87–128.

Hussein M I 2009 *in* 'Proceedings of the Royal Society of London A: Mathematical, Physical and Engineering Sciences' Vol. 465 The Royal Society pp. 2825–2848.

Joannopoulos J D, Johnson S G, Winn J N & Meade R D 2011 *Photonic crystals: molding the flow of light* Princeton university press.

Kushwaha M S, Halevi P, Dobrzynski L & Djafari-Rouhani B 1993 *Physical Review Letters* **71**(13), 2022.

Leung K & Liu Y 1990 *Physical Review Letters* **65**(21), 2646.

Lu Y & Srivastava A 2016 *Wave Motion* **60**, 46–61.

Milton G W & Willis J R 2007 *Proceedings of the Royal Society A: Mathematical, Physical and Engineering Science* **463**(2079), 855–880.

Minagawa S & Nemat-Nasser S 1976 *International Journal of Solids and Structures* **12**(11), 769–777.

Minagawa S, Nemat-Nasser S & Yamada M 1981 *International Journal for Numerical Methods in Engineering* **17**(9), 1335–1353.

Nemat-Nasser S 1972*a* *Journal of Elasticity* **2**(2), 73–90.

Nemat-Nasser S 1972*b* *Journal of Applied Mechanics* **39**, 850.

Nemat-Nasser S 2015*a* *in* 'Proc. R. Soc. A' Vol. 471 The Royal Society p. 20150152.

Nemat-Nasser S 2015*b* *Acta Mech. Sin.* **31**, 481–493.

Nemat-Nasser S, Fu F & Minagawa S 1975 *International Journal of Solids and Structures* **11**(5), 617–642.

Nemat-Nasser S & Srivastava A 2011 *Journal of the Mechanics and Physics of Solids* **59**(10), 1953–1965.

Nemat-Nasser S, Willis J R, Srivastava A & Amirkhizi A V 2011 *Physical Review B* **83**(10), 104103.

Pendry J 1994 *Journal of Modern Optics* **41**(2), 209–229.

Pendry J B 1996 *Journal of Physics: Condensed Matter* **8**(9), 1085.

Plihal M & Maradudin A 1991 *Physical Review B* **44**(16), 8565.

Sengupta L C & Sengupta S 1999 *Material Research Innovations* **2**(5), 278–282.

Si W, Cruz E, Johnson P, Barnes P W, Woodward P & Ramirez A 2002 *arXiv preprint cond-mat/0205153* .

Siddiqui O F, Mojahedi M & Eleftheriades G V 2003 *Antennas and Propagation, IEEE Transactions on* **51**(10), 2619–2625.

Srivastava A 2015 *International Journal of Smart and Nano Materials* **6**(1), 41–60.

Srivastava A & Nemat-Nasser S 2012 *Proceedings of the Royal Society A: Mathematical, Physical and Engineering Science* **468**(2137), 269–287.

Sukhovich A, Jing L & Page J H 2008 *Physical Review B* **77**(1), 014301.

Tran P 1995 *Physical Review B* **52**(15), 10673.

Willis J 1981*a* *Advances in applied mechanics* **21**, 1–78.

Willis J 1981*b* *Wave Motion* **3**(1), 1–11.

Willis J 1984 *Wave Motion* **6**(2), 127–139.

Willis J 2009 *Mechanics of Materials* **41**(4), 385–393.

Wing Z N, Halloran J W, Gong X, She W H, Hoppenjans E & Chappell W J 2006 *Journal of the American Ceramic Society* **89**(9), 2812–2815.

Yablonovitch E, Gmitter T & Leung K 1991 *Physical review letters* **67**(17), 2295.

Yang M, Ma G, Wu Y, Yang Z & Sheng P 2014 *Physical Review B* **89**(6), 064309.

Zhang L, Mumcu G, Yarga S, Sertel K, Volakis J L & Verweij H 2008 *Journal of Materials Science* **43**(5), 1505–1509.

Zhang X & Wu Y 2015 *Scientific reports* **5**.